HAL
open science

How to position sensors in thermo-acoustic tomography?

Maïtine Maïtine Bergounioux, Elie Bretin, Yannick Privat

To cite this version:

Maïtine Maïtine Bergounioux, Elie Bretin, Yannick Privat. How to position sensors in thermo-acoustic tomography?. Inverse Problems, 2019, 35 (7), pp.074003. 10.1088/1361-6420/ab0e4d . hal-01874889v2

HAL Id: hal-01874889

https://hal.science/hal-01874889v2

Submitted on 6 Mar 2019

HAL is a multi-disciplinary open access archive for the deposit and dissemination of scientific research documents, whether they are published or not. The documents may come from teaching and research institutions in France or abroad, or from public or private research centers.

L'archive ouverte pluridisciplinaire **HAL**, est destinée au dépôt et à la diffusion de documents scientifiques de niveau recherche, publiés ou non, émanant des établissements d'enseignement et de recherche français ou étrangers, des laboratoires publics ou privés.

How positioning sensors in thermo-acoustic tomography?*

Maïtine Bergounioux† Élie Bretin‡ Yannick Privat§

March 4, 2019

Abstract

Thermo-acoustic tomography is a non-invasive medical imaging technique: the object to be reconstructed is excited by an impulse, inducing inhomogeneous heating and thus tissue expansion. This creates an acoustic wave pressure that can be measured by sensors. The reconstruction of internal heterogeneities can then be achieved by solving an inverse problem, once the sound wave measurements are known outside the body. As the measured pressure intensity is expected to be low, a difficult problem is to position the sensors properly.

This article is devoted to determining the positions of the sensors in order to carry out the reconstruction procedure in an optimal way. We first introduce a model of optimal sensor position that involves a deviation function between the theoretical pressure and the measured pressure for a first series of sensor measurements, and a constant observable type function that describes the quality of reconstruction. We use it to determine an *appropriate* position of the sensors for a second set of measurements.

Far from providing an intrinsic solution to the general issue of positioning sensors, solving this problem makes it possible to obtain a new position of the sensors improving the quality of the reconstruction before obtaining a new series of measurements.

This model is analyzed mathematically: we study the existence problems and introduce a numerical algorithm to solve them. Finally, several 2D numerical simulations illustrate our approach.

Keywords: wave equation, observability, shape optimization, calculus of variation, minimax problem, primal-dual algorithm.

AMS classification: 49J20, 35M33, 80A23, 93C20.

*Y. Privat was partially supported by the Project "Analysis and simulation of optimal shapes - application to lifesciences" of the Paris City Hall.

†Institut Denis Poisson, Université d'Orléans, CNRS UMR 7013, 45067 Orléans, France (maitine.bergounioux@univ-orleans.fr).

‡Univ Lyon, INSA de Lyon, CNRS UMR 5208, Institut Camille Jordan, 20 avenue Albert Einstein, F-69621 Villeurbanne Cedex, France (elie.bretin@insa-lyon.fr)

§IRMA, Université de Strasbourg, CNRS UMR 7501, 7 rue René Descartes, 67084 Strasbourg, France (yannick.privat@unistra.fr).

1 Introduction

In this article, we focus on thermo-acoustic tomography, a non-invasive medical imaging technique that seems very promising because, compared to other imaging techniques such as X-ray tomography or emission tomography, it is based on simple and relatively inexpensive equipment. It is particularly well suited for low-density tissue imaging and is likely to become a major tool for mammography and even brain imaging. The development of non-invasive and non-ionizing imaging techniques is particularly important for the early detection of breast cancer in young patients, whose mammograms are generally of low contrast. The principle of this imaging process is very simple: the tissue to be visualized is irradiated by a pulse and this energy induces a heating process. If the pulse is an electromagnetic radio-frequency pulse, the technique is called thermo-acoustic tomography (TAT); if the pulse is a laser (the frequency is much higher), it is called photo-acoustic tomography (PAT). In any case, this creates a thermally induced pressure surge that propagates as a sound wave, which can be detected by sensors located outside the body to image. By detecting pressure waves, heterogeneities can be observed: this gives important information such as the position and/or size of tumors in breast cancer. For more details on the process and related work, we refer to [1, 11, 12, 25] and the references contained therein. Basically, TAT and PAT are two hybrid techniques using electromagnetic waves as excitation (input) and acoustic waves as observation (output). Both techniques lead to similar misplaced reverse problems. The modeling of the direct problem does not lead to the same equations, since the physical background is not the same. However, the process can be described using two equations (or systems of equations):

- The first system of equations describes the generation of the heating process inside the body; in PAT, this system involves the fluence equation (the fluence rate is the average of the light intensity in all directions) which is a diffusion equation [11] whereas in TAT, this equation is replaced by the Maxwell equations [1]. Temperature is described by the classical thermal equation, which can be neglected in PAT since the high speed of light implies that the thermal effect is *almost instantaneous*. In both cases, the resulting term is a source pressure wave p_0 at the time $t = 0$.

- The second equation models the behaviour of the acoustic wave once the source p_0 is known. It writes

$$\begin{cases} \partial_{tt} p(t,x) - \operatorname{div}(c(x)\nabla p(t,x)) = 0 & \text{in } (0,T)\times\mathcal{B}, \\ p(0,\cdot) = p_0, & \text{on } \mathcal{B}, \\ \partial_t p(0,\cdot) = 0 & \text{on } \mathcal{B}, \\ p = 0 & \text{on } (0,T)\times\partial\mathcal{B}, \end{cases} \tag{1.1}$$

  where $T > 0$ is arbitrary and $\mathcal{B}$ is a given ball whose radius will be chosen appropriately in the sequel. Most articles on the subject have focused on this second equation to address inversion. Indeed, if measurements are made to determine p_0, then the heterogeneities can be identified by quantitative estimates of two appropriate physical parameters: diffusion and absorption coefficients in PAT, or electrical sensitivity and conductivity in TAT.

In this article, we focus on the following question:

from the knowledge of a first series of measurements, how to locate the sensors before performing a second one, in a relevant way?

Such a question is related to the general problem of optimal sensor positioning. In the following, we focus on the pressure equation to obtain the best reconstruction of p_0. The future analysis can be used interchangeably in both PAT and TAT frameworks. In the following, we always refer to the TAT process for readability reasons.

Our goal is therefore to determine the position of the sensors providing the best possible reconstruction. As a result, we do not focus on solving the inverse problem (where the sensors are fixed). Many articles on TAT/PAT reconstruction have been written in recent decades. For example, we refer to [1, 7, 8, 9, 11, 12, 25, 33] and to the book by Ammari et al. [3, 6] or Scherzer et al. [31].

To our knowledge, the question of the optimal positioning of the sensors has not yet been addressed in the context of photoacoustic tomography. However, it can be noted that the search for the optimal position and/or shapes of the sensors for the wave/heat equation in a delimited domain has been studied in [26, 27, 28, 29, 30]. In these articles, it is assumed that, in a certain sense, a phenomenon of reflection of solutions at the boundary of the domain occurs. Such an assumption is not relevant for the application we are considering here and we propose an alternative approach. Also worth mentioning is [2, 4], where the issue of recovering small inhomogeneities of conductivity in a homogeneous background medium from dynamic boundary measurements over a part of the boundary and over a finite time interval is addressed. These problems differ from those studied here, since the proposed reconstruction algorithm depends on particular choices of initial data and boundary conditions. In the following, we basically look for the initial data and optimal sensor positions at the same time, which requires a dedicated method.

Another related problem is the optimization of electrode positions in electrical impedance tomography, which aims to retrieve information on electrical conductivity within a physical body from current and potential boundary measurements. The optimal electrode locations are determined so that, taking into account the measurement, the conditional conductivity density is as localized as possible (see for example [17, 20, 23, 24, 34]). Nevertheless, a huge difference between this work and the present paper lies in the physical model itself. The modeling and approaches studied in our paper are adapted to the wave equation model. Indeed, we will use a certain observability constant to define the functional cost, time inversion techniques to solve the resulting problem numerically, etc.

In the following, the determination of the optimal position or shape of the sensors will be addressed in two ways:

(i) **First attempt: prescription of the total surface area of the sensors.** We first choose to process sensors described by the characteristic function of a measurable subset whose Lebesgue measurement is prescribed. A possible disadvantage of such

an approach is that the optimal solution may not exist or may have a high/infinite number of connected components (see problem (2.13)).

(ii) **Second attempt: prescription of the maximum number of sensors.** To avoid the emergence of overly complex solutions and to make problem modeling more realistic, we will examine a second point of view where a maximum number of N_0 of sensors (specifically connected components of the sensor set) is prescribed, in addition to the total surface mentioned above (see Problem (2.21)).

The document is organized as follows: Section 2 is dedicated to problem modeling. We justify here the point of view adopted. In the section 3, we analyze the problem of optimization, in particular the problems of existence and deduce the optimal conditions. Finally, the 4 section is devoted to describing a numerical algorithm and presenting the first promising numerical results.

2 Modeling the problem

2.1 The PDE (direct) model and the sensors set

Throughout this paper, we will use the notation $\mathbb{1}_A$ as the characteristic function of a set $A \subset \mathbb{R}^d$ $(d \geq 1)$ which is the function equal to 1 on A and 0 elsewhere.

As explained in Section 1, the acoustic wave is assumed to solve the partial differential equation

$$\begin{cases} \partial_{tt} p(t,x) - \operatorname{div}(c(x)\nabla p(t,x)) = 0 & \text{in } (0,T)\times\mathcal{B}, \\ p(0,\cdot) = p_0, & \text{on } \mathcal{B}, \\ \partial_t p(0,\cdot) = 0 & \text{on } \mathcal{B}, \\ p = 0 & \text{on } (0,T)\times\partial\mathcal{B}, \end{cases} \tag{2.1}$$

where $T > 0$ is arbitrary and $\mathcal{B} \subset \mathbb{R}^d$ is a given ball whose radius R is chosen in the sequel.

Let us also introduce Ω as a convex open subset of $\mathbb{R}^d$, representing the body to image, which means in particular that

$$\operatorname{supp}(p_0) \subset \Omega, \tag{2.2}$$

where $\operatorname{supp}(p_0)$ denotes the support of p_0. The convexity assumption on Ω is technical, and will be used to make the set of admissible designs well defined in the sequel. This will be commented later.

For this reason, we assume that $\mathcal{B}$ is large enough so that $\Omega \subset \mathcal{B}$; the set $\mathcal{B} \setminus \Omega$ stands for the ambient media (water or air), where the wave propagates.

The function $c \in L^\infty(\mathbb{R}^d)$ stands for the sound speed and satisfies

$$c(x) \geq c_0 > 0 \quad \text{a.e. } x \in \mathbb{R}^d.$$

A typical choice for c is to assume it is piecewise constant, namely:

$$c = c_1 \mathbb{1}_\Omega + c_2 \mathbb{1}_{\mathcal{B}\setminus\Omega}, \quad \text{with } (c_1, c_2) \in (\mathbb{R}_+^*)^2, \tag{2.3}$$

with $c_1,\ c_2 > 0$. Recall that for every initial $p_0 \in H_0^1(\Omega)$, there exists a unique solution p to System (2.1) and that solution satisfies $p \in \mathcal{C}^1\left([0,T], L^2(\mathcal{B})\right) \cap \mathcal{C}^0\left([0,T], H_0^1(\mathcal{B})\right)$ (see e.g. [16, 19]).

Remark 2.1. For (future) numerical purposes, we choose $\mathcal{B}$ as a bounded ball with radius R. However, R is large enough, then p vanishes on $\partial\mathcal{B}$ all along the recording process (i.e. for $t \leqslant T$). Precisely, there exists $R > 0$ large enough such that, for every $p_0 \in H_0^1(\Omega)$, the solution of problem (2.1) coincides with the solution of

$$\begin{cases} \partial_{tt} p(t,x) - \operatorname{div}(c(x)\nabla p(t,x)) = 0 & \text{in } (0,T)\times \mathbb{R}^d, \\ p(0,\cdot) = p_0(\cdot) & \text{on } \mathbb{R}^d, \\ \partial_t p(0,\cdot) = 0 & \text{on } \mathbb{R}^d, \end{cases} \tag{2.4}$$

with the convention that the initial datum p_0 has been extended by 0 to the whole space $\mathbb{R}^d$. One refers for instance to [19].

As mentioned in Section 1, the inverse problem of recovering $p_0 \in H_0^1(\Omega)$ from p measurements on a set $(0,T)\times\Sigma$ (where Σ is the position of the sensors) has been extensively studied over the past two decades. We refer to [3, 6, 11, 12, 25] and the references therein for more details. However, the point of view we adopt here is a variational one. Specifically, we do not use a reconstruction formula (exact or not) or a time inversion approach. to deal with the inverse problem. Following the philosophy of [1, 11, 12], we rather include the unknown parameter in a cost functional. As a result, the reconstruction of p_0 and the question of the position of the sensors will be addressed in terms of functional minimization.

The sensors set. To model the sensors optimal positioning, we first describe the class of admissible designs/sensors to be considered.

Let us endow the Lipschitz set $\partial\Omega$ with the usual $(d-1)$-dimensional Hausdorff measure $\mathcal{H}^{d-1}$. In the sequel, we say by convention that $\Gamma \subset \partial\Omega$ is measurable whenever it is measurable for the Hausdorff measure $\mathcal{H}^{d-1}$.

Introduce $\Sigma \subset \mathbb{R}^d$ as the subdomain of $\mathbb{R}^d$ occupied by sensors. Roughly speaking, we will assume that every connected component of Σ is located around the boundary of Ω and has a positive *thickness* ε. Precisely, we assume the existence of a measurable set $\Gamma \subset \partial\Omega$ such that

$$\Sigma = \{s + \mu\,\nu(s), s \in \Gamma, \mu \in [0,\varepsilon]\}\,, \tag{2.5}$$

where $\nu(s)$ denotes the outward unit normal to Ω at s (see Figure 2.1). The set Σ is thus supported by the annular ring

$$\widetilde{\partial\Omega} := \{s + \mu\nu(s), s \in \partial\Omega, \mu \in [0,\varepsilon]\}.$$

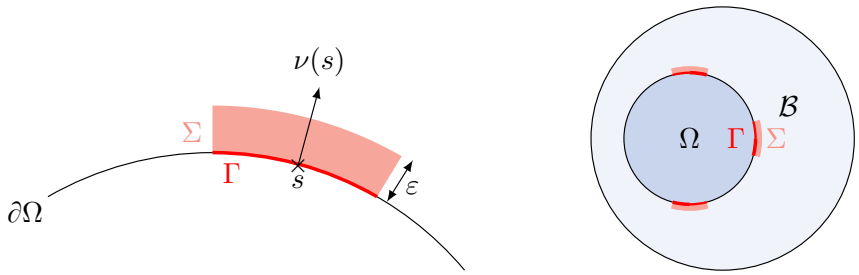

Figure 2.1: The set of sensors.

Remark 2.2. In this work, we have chosen to treat volumetric sensors: this will determine the choice of the term observability in the cost functional. Another relevant model could be that of boundary sensors, which would imply changing the choice of the above observability term in the cost functional.

When investigating the optimal position or shape of sensors without any restriction on the sensors domain measure, the solution is trivial and is given by $\Sigma = \widetilde{\partial\Omega}$ (see e.g. [26, 27, 28, 29, 30]). This is not relevant for practical purposes and this is why we also assume in the sequel that the measure of the sensors domain is prescribed: the measurable subsets Γ of $\partial\Omega$ satisfy $\mathcal{H}^{d-1}(\Gamma) = L\mathcal{H}^{d-1}(\partial\Omega)$, where $L \in (0,1)$ denotes some given real number. Let us introduce the two classes

$$\mathcal{V}_L = \{a \in L^\infty(\partial\Omega),\ a \in \{0,1\},\ \text{a.e. in } \partial\Omega,\ \int_{\partial\Omega} a(x)d\mathcal{H}^{d-1}(x) = L\mathcal{H}^{d-1}(\partial\Omega)\}. \tag{2.6}$$

of admissible subsets $\Sigma \subset \mathcal{B}$ characteristic functions and

$$\mathcal{U}_L = \{a \in L^\infty(\widetilde{\partial\Omega}),\ a(s+\mu\nu(s)) = X(s),\ \ \text{a.e. } (s,\mu) \in \partial\Omega \times [0,\varepsilon],\ \text{with } X \in \mathcal{V}_L\} \tag{2.7}$$

of admissible subsets $\Gamma \subset \widetilde{\partial\Omega}$ characteristic functions.

Since Ω is assumed to be convex, the set $\mathcal{U}_L$ well defined. Indeed, Ω has in particular a Lipschitz boundary and the normal outward vector $\nu(\cdot)$ exists almost everywhere on $\partial\Omega$. The convexity assumption implies that the map $\widetilde{\partial\Omega} \ni s + \mu\nu(s) \mapsto (s,\mu) \in \partial\Omega \times [0,\varepsilon]$ is invertible according to the projection on a convex set theorem.

2.2 Criteria choices and optimization problems

In this section, we model the problem by describing the cost functional and set the optimization problems. Let $p_{obs} \in L^2((0,T)\times\Sigma)$ denote the measured pressure: it is defined in $(0,T)\times\Sigma$. We extend p_{obs} by 0 to $(0,T)\times\mathcal{B}$ and denote the obtained function similarly, with

a slight abuse of notation. Hence, one has $p_{obs} = \mathbb{1}_\Sigma p_{obs}$ so that $p_{obs} \in L^2(0,T,L^2(\mathcal{B}))$. For $p_0 \in H_0^1(\Omega)$, we also introduce $p_{[p_0]}$ as the solution of Problem (2.1) for the initial datum p_0.

The issue we are now addressing is as follows: **given a first (series of) measurement(s), how can we determine a relevant sensor position before performing a new (series of) measurement(s)?**
To achieve this objective, we introduce an optimal design problem. Our approach can be split into two steps that we roughly describe.

- **First step: determination of an initial pressure condition p_0.** Recall that, in the PDE model we consider (see Eq. (2.1)), the initial velocity is assumed to vanish identically in $\mathcal{B}$. It is therefore enough to reconstruct the initial pressure. A first natural (naive) idea would be to consider the problem

$$\inf_{p_0 \in \mathcal{P}_0(\Omega)} A_1(\mathbb{1}_\Sigma, p_0) \tag{2.8}$$

where

$$A_1(\mathbb{1}_\Sigma, p_0) := \frac{1}{2}\int_0^T \int_{\mathcal{B}} \mathbb{1}_\Sigma(x)(p_{[p_0]}(t,x) - p_{obs}(t,x))^2 \, dx \, dt. \tag{2.9}$$

and $\mathcal{P}_0(\Omega)$ is a given functional space to be chosen adequately in the sequel. Unfortunately, the well-posedness of such least square problems, is in general not ensured. In addition, due to the uncertainties of sensor measurements and the fact that Σ is a strict sub-domain of $\widetilde{\partial\Omega}$, there could be many initial pressures of p_0 leading to the observation p_{obs}. Therefore, we decide to select an initial pressure function denoted $\widetilde{p_0}$ by solving a penalized optimization problem in order to impose three kinds of physical constraints: we look for (i) positive pressure term, (ii) whose support is included in a fixed compact set K of $\mathcal{B}$, and (iii) belonging to a functional space well-chosen to ensure the well-posedness of the problem and therefore good reconstruction properties. From a practical viewpoint, this will be done adding a penalization-regularization term denoted $\mathcal{R}(p_0)$ in the definition of the criterion. The choice of such a term will be introduced and commented in Section 3.1.

  Solving the resulting problem (see its definition below) is a way to define an initial pressure function reconstructed (almost) everywhere in $\mathcal{B}$ and not only on Σ. This is the key point to address the optimal design problem in the second step.

- **Second step: determination of the best position of sensors.** Once an initial pressure $\widetilde{p_0}$ has been determined with a given position of sensors, the new position will be obtained by solving the optimal design problem

$$\sup_{\mathbb{1}_\Sigma \in \mathcal{U}_L} A_2(\mathbb{1}_\Sigma, p_0),$$

where

$$A_2(\mathbb{1}_\Sigma, p_0) := \frac{\int_0^T \int_{\mathcal{B}} \mathbb{1}_\Sigma(x) \partial_t p_{[\widetilde{p_0}]}(t,x)^2 \, dx \, dt}{\|p_0\|^2_{H^1(\Omega)}}. \tag{2.10}$$

The functional to maximize represents the quality of the observation: we discuss and comment on such a choice below. In summary, we are looking for the position of the sensors allowing the best observation of the worst possible pressure p_0 leading to the observation p_{obs}.

To summarize, this two step procedure leads to the following optimal design problem:

Optimal position of sensors (new version). Let $p_{obs} \in L^2(\Sigma)$ and $\gamma \in \mathbb{R}_+^*$ be a fixed parameter.

1. Computation of an initial pressure function $\widetilde{p}_0$ (whenever it exists) by solving the problem
$$\inf_{p_0 \in \mathcal{P}_0(\Omega)} J^0(\mathbb{1}_\Sigma, p_0), \tag{2.11}$$
where the cost-functional J^0 is defined by
$$J^0(\mathbb{1}_\Sigma, p_0) = A_1(\mathbb{1}_\Sigma, p_0) + \gamma \mathcal{R}(p_0), \ \gamma > 0 \tag{2.12}$$
and the admissible set is
$$\mathcal{P}_0(\Omega) = \{p_0 \in L^2(\Omega) \mid \mathrm{supp}(p_0) \subset K, \ p_0 \geqslant 0 \text{ a.e. in } \Omega \text{ and } \mathcal{R}(p_0) < +\infty\},$$
where $\mathcal{R}(p_0)$ is a penalization-regularization term whose choice will be made precise in Section 3.1.

2. Assuming that Problem (2.11) has a solution $\widetilde{p}_0$, determination of a new sensors position by solving
$$\sup_{\mathbb{1}_\Sigma \in \mathcal{U}_L} A_2(\mathbb{1}_\Sigma, \widetilde{p}_0) \tag{2.13}$$

Next, to deal with more realistic constraints, we introduce a modified optimal design problem, where then sensors set is assumed to be the union of connected components N_0 having the same length, N_0 being a given non-zero integer. For simplicity's sake, we will assume that the dimension of the space is $d = 2$ and that the boundary of the convex set Ω is smooth, say $\mathcal{C}^1$.. Let O denote any point of Ω and assume that Ω has as polar equation $r = \rho(\theta)$ in a given orthonormal basis of $\mathbb{R}^2$ centered at O, where ρ is a Lipschitz function of the one-dimensional torus $\mathbb{T} = \mathbb{R}/[0, 2\pi)$.

Let us make this sensors set precise. Let $\ell > 0$ be such that $\ell N_0 < \int_{\mathbb{T}} \sqrt{\rho(\theta)^2 + \rho'(\theta)^2}\, d\theta$. We choose to consider the set of sensors represented by $\Sigma \subset \widetilde{\partial\Omega}$ associated to the domain Γ with $\mathbb{1}_\Gamma \in \mathcal{V}_L$ through the formula (2.7)-(2.6), parametrized by a nondecreasing family $(\theta_n)_{n \in \{1,\dots,N_0\}} \in \mathbb{T}^{N_0}$ such that Σ is associated to Γ by the relation
$$\mathbb{1}_\Sigma(x) = \mathbb{1}_\Gamma(s + \mu\nu(s)) = \mathbb{1}_\Gamma(s), \qquad \text{for a.e. } x \in \widetilde{\partial\Omega}, \ s \in \partial\Omega, \ \mu \in [0, \varepsilon] \tag{2.14}$$

for some $\mathbb{1}_\Gamma \in \mathcal{V}_L$, where

$$\Gamma = \bigcup_{n=1}^{N_0} \Gamma_n \qquad \text{with} \qquad \Gamma_n = \{(r\cos\theta, r\sin\theta) \in \Gamma \mid \theta \in (\theta_n, \hat{\theta}_n)\}, \tag{2.15}$$

where $\hat{\theta}_n$ is defined from θ_n by the relation

$$\int_{\theta_n}^{\hat{\theta}_n} \sqrt{\rho(s)^2 + \rho'(s)^2}\, ds = \ell. \tag{2.16}$$

Note that, since the mapping $\mathbb{T} \ni \theta \mapsto \int_{\theta_n}^{\hat{\theta}_n} \sqrt{\rho(s)^2 + \rho'(s)^2}\, ds$ is continuous and monotone increasing, it defines a bijection. This justifies the consistence of definition of $\hat{\theta}_n$ by (2.16). Basically, the last equality requires that all sensors be represented by N_0 of almost identical connected components (up to isometrics).

To avoid the overlapping of sensors, we will also require that

$$\forall n \in \{1, \dots, N_0 - 1\}, \qquad \hat{\theta}_n \leqslant \theta_{n+1}. \tag{2.17}$$

It will be useful for the upcoming analysis to note that this last condition will rewrite

$$\forall n \in \{1, \dots, N_0 - 1\}, \qquad \int_{\theta_n}^{\theta_{n+1}} \sqrt{\rho(s)^2 + \rho'(s)^2}\, ds \geqslant \ell. \tag{2.18}$$

As a conclusion, we will restrict the set of admissible configurations to

$$\mathcal{U}_{L,N_0}^{\ell} = \{\mathbb{1}_\Sigma \in \mathcal{U}_L \mid \Sigma \text{ associated to } \Gamma \text{ by (2.14) with } \mathbb{1}_\Gamma \in \mathcal{V}_{L,N_0}^{\ell}\}, \tag{2.19}$$

where

$$\mathcal{V}_{L,N_0}^{\ell} = \{\mathbb{1}_\Gamma \in \mathcal{V}_L \mid \Gamma \text{ satisfies (2.15)-(2.16)-(2.18)}\}. \tag{2.20}$$

Optimal position of sensors (updated version with a maximal number of connected components). Let $N_0 \in \mathbb{N}^*$, $\ell > 0$ such that $\ell N_0 < \int_0^{2\pi} \sqrt{\rho(\theta)^2 + \rho'(\theta)^2}\, d\theta$, $p_{obs} \in L^2(\Sigma)$ and $\gamma \in \mathbb{R}_+^*$ be a fixed parameter.

1. Computation of an initial pressure function $\widetilde{p}_0$ (whenever it exists) by solving the problem (2.11) (as for the optimal design problem (2.13)).

2. Assuming that Problem (2.11) has a solution $\widetilde{p}_0$, determination of a new sensors position by solving

$$\sup_{\mathbb{1}_\Sigma \in \mathcal{U}_{L,N_0}^{\ell}} A_2(\mathbb{1}_\Sigma, \widetilde{p}_0), \tag{2.21}$$

where $\mathcal{U}_{L,N_0}^{\ell}$ is given by (2.19).

In the section 4, we will discuss this method and illustrate it with several numerical results.

Comments on the terms A_1 and A_2. We end this section with comments on the choice of the functional.

The term $A_1(\mathbb{1}_\Sigma, p_0)$ is a *least-square* fidelity term, ensuring that the initial pressure p_0 makes the pressure $p_{[p_0]}$ (corresponding to the reconstructed image) as close as possible to the observed pressure p_{obs} on the domain occupied by sensors. The term $A_2(\mathbb{1}_\Sigma, p_0)$ is inspired by the notion of *observability* in the theory of control or inverse problems. Indeed, the equation (2.1) is said to be *observable in time T on Σ* if there is a positive constant C such that the inequality

$$C\|p_0\|^2_{H^1_0} \leqslant \int_0^T \int_{\mathcal{B}} \mathbb{1}_\Sigma(x) \left|\partial_t p_{[p_0]}(t,x)\right|^2 \, dxdt, \tag{2.22}$$

holds for every initial datum $p_0 \in H^1_0(\Omega)$. The largest constant $C = C_T(\mathbb{1}_\Sigma)$ such that the inequality (2.22) holds is the so-called *observability constant* and writes

$$C_T(\mathbb{1}_\Sigma) = \inf_{p_0 \in H^1_0(\mathcal{B})} \frac{\int_0^T \int_{\mathcal{B}} \mathbb{1}_\Sigma(x) \left|\partial_t p_{[p_0]}(t,x)\right|^2 \, dx\, dt}{\|p_0\|^2_{H^1_0}}.$$

This constant $C_T(\mathbb{1}_\Sigma)$ gives an idea of the well-posed character of the p_0 reconstruction from measurements of $p_{[p_0]}$ on Σ. In short, the higher the observability constant, the better the quality of the reconstruction.

The functional A_2 thus models the efficiency of a set of sensors occupying the Σ domain. It should also be noted that the choice of the observation variable $\mathbb{1}_\Sigma \partial_t p_{[p_0]}$ is determined by the fact that the sensors are generally piezoelectric microphones, which are supposed to record temporal pressure variations.

Finally, to understand the role of maximization with respect to the position of the sensors, we have illustrated a a *bad* situation on Figure 2.2; here a sensors position on a domain Σ_2 gives a less precise result than another position on a subdomain Σ_1, since the observed pressure coincides only with the real one on the domain Σ_2. Maximization with respect to design can then be interpreted as a functional *worst case* function, used to move the sensors to a position ignored by previous measurements and where the reconstructed pressure is far from that observed.

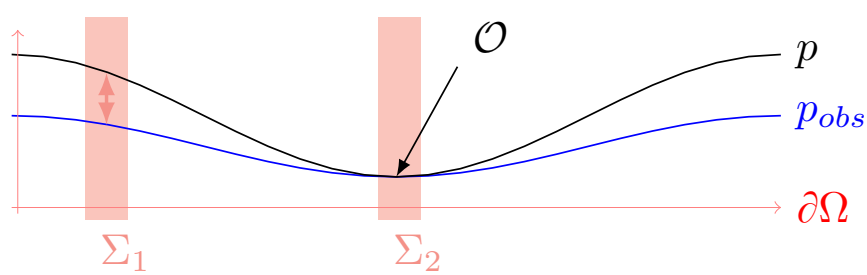

Figure 2.2: A bad situation.

3 Analysis of Problems (2.11) and (2.13)

3.1 Choice of the regularization term $\mathcal{R}(p_0)$

Let's add some comments to fully specify the model (via the cost functional). If we consider Problem (2.8), it is clear that the ill-posedness of this problem prevents a solution from being found (to highlight such a claim, one can easily build counterexamples based on gaussian beams). Therefore, it is necessary to define a coercive cost functional in relation to the functional space by adding a penalty-regularization term $\mathcal{R}(p_0)$.

- If we decide to choose $L^2(\mathcal{B})$, as initial pressure space, we ask for the weakest regularity. In that case $\mathcal{R}(p_0) = \|p_0\|_{L^2}$. This implies that p_0 may be small since the first term only involves "sparse" observation of p and is expected to be small even for small ε.

- We hope to recover the heterogeneities as images with sharp edges, which can be captured adequately by considering the functions of bounded variation. Indeed, the involvement of the first derivative via the total variation has a noise-reducing effect. However, to our knowledge, the solution of the wave equation with the BV data is not standard. For this reason, in the upcoming analysis, we prefer to process more regular data and choose a penalization functional that induces a H^1-smoothing effect. Therefore, we expect to recover diffuse objects. To avoid a too hard regularization process, we also use the $W^{1.1}$ standard (which is the same as TV-one in this case).

- Finally, we don't have any compactness result to achieve the convergence process of subsequences. Therefore, we add a (small) viscosity penalization term which must rather be interpreted as a theoretical tool.

Eventually, we choose

$$\boxed{\mathcal{R}(p_0) = \|\nabla p_0\|_{L^1} + \frac{\varepsilon}{2\gamma}\|p_0\|^2_{H^1}}, \tag{3.1}$$

so that the cost functional reads

$$J(p_0) := A_1(\mathbb{1}_\Sigma, p_0) + \gamma\|\nabla p_0\|_{L^1} + \frac{\varepsilon}{2}\|p_0\|^2_{H^1}, \tag{3.2}$$

where $\varepsilon \ll \gamma$ and $A_1(p_0) = A_1(\mathbb{1}_\Sigma, p_0)$ is given by (2.9). Throughout this section, we omit the dependence with respect to Σ since this set is fixed. Hence, Problem (2.11) can be written as

$$\inf_{p_0 \in \mathcal{P}_K(\Omega)} J(p_0), \tag{3.3}$$

where K is a fixed compact subset of Ω and

$$\mathcal{P}_K(\Omega) = \{p_0 \in H^1_0\Omega) \mid \mathrm{supp}(p_0) \subset K \text{ and } p_0 \geqslant 0 \text{ a.e. in } \Omega\}.$$

Note that $\mathcal{P}_K(\Omega)$ is convex and closed for the weak $H^1(\Omega)$-topology.

Remark 3.1. *Typically, we choose $K := \{x \in \Omega \mid d(x, \partial\Omega) \geq \delta\ \}$ for some positive parameter δ.*

3.2 Analysis of Problem (3.3)

In the sequel we denote by bold letters functions that are defined on $(0,T)\times\mathcal{B}$. Precisely, for any $p\in H^1_0(\Omega)$, we denote $\mathbf{p}$ the solution of (2.1) where $\mathbf{p}(\mathbf{0},\cdot)$=$p$.

Existence and uniqueness.

Theorem 3.1. *Fix $\varepsilon>0$ and $\gamma>0$. Then problem (3.3) has a unique solution p^*.*

Proof. Let $(p_n)_{n\in\mathbb{N}}$ be a minimizing sequence of (3.3). Therefore, $(p_n)_{n\in\mathbb{N}}$ is weakly convergent to some p_0 in $H^1(\Omega)$ and $W^{1,1}(\Omega)$ and strongly in $L^2(\Omega)$. As $\mathcal{P}_K(\Omega)$ is $H^1(\Omega)$ weakly closed then $p_0\in\mathcal{P}_K(\Omega)$. Moreover, the sequence $(\mathbf{p_n})_{n\in\mathbb{N}}$ defined by $\mathbf{p_n}:=p_{[p_n]}$ strongly converges to $\mathbf{p_0}:=p_{[p_0]}$ in $L^\infty\left([0,T],L^2(\mathcal{B})\right)$ (see [16, Theorem 2 p. 567]). According to the Lebesgue theorem, we infer that $A_1(p_n)\to A_1(p_0)$ as $n\to+\infty$. We end the proof with the lower semi-continuity of the norms in the regularizing term. Uniqueness is an easy consequence of the strict convexity of the H^1-norm. Note that the $\|p_0\|^2_{H^1}$ term is used both for existence and uniqueness. □

Optimality conditions. Let p^* be the solution to (3.3) and (as before) $\mathbf{p}^*$ the solution of (2.1) where $\mathbf{p}^*(0,\cdot)=p^*$ and look for optimality conditions. For every $p\in\mathcal{P}_K(\Omega)$ we get

$$0\in\partial J(p^*),$$

where $\partial J(p^*)$ stands for the subdifferential of J at p^* (see [18] for example). Indeed, J is not Gâteaux-differentiable because of the TV term. This yields

$$-D[A_1](p^*)-\varepsilon(p^*-\Delta p^*)\in\gamma\partial TV(p^*). \tag{3.4}$$

Recall that $TV(p^*)=\|\nabla p^*\|_{L^1}$ since $p^*\in H^1_0(\Omega)$ but we use this notation for convenience. We first compute $D[A_1](p^*)$ (the derivative with respect to p^*) by introducing an adjoint state. Let us define $\mathbf{q}^*$ as the solution of

$$\begin{cases} \partial_{tt}\mathbf{q}^*(t,x)-\mathrm{div}(c(x)\nabla\mathbf{q}^*(t,x))=(\mathbf{p}^*(t,x)-p_{obs}(t,x)))\mathbb{1}_\Sigma(x) & \text{in } (0,T)\times\mathcal{B},\\ \mathbf{q}^*(T,\cdot)=0,\ \partial_t\mathbf{q}^*(T,\cdot)=0 & \text{on } \mathcal{B},\\ \mathbf{q}^*=0 & \text{on } (0,T)\times\partial\mathcal{B}, \end{cases} \tag{3.5}$$

For every $p\in H^1_0(\Omega)$, a simple computation yields

$$D[A_1](p^*)\cdot p=\int_0^T\int_{\mathcal{B}}\mathbb{1}_\Sigma(x)(\mathbf{p}^*(t,x)-p_{obs}(t,x))\,\mathbf{p}(t,x)dx\,dt.$$

Indeed, by linearity, the derivative of $p_0\mapsto p_{[p_0]}$ with respect to p_0 is $p_{[p_0]}$. Using (3.5) and two integrations by parts, we get

$$D[A_1](p^*)\cdot p=-\int_{\mathcal{B}}\mathbb{1}_\Sigma(x)\,\mathbf{q}^*(0,x)p(x)\,dx\ ,$$

so that $D[A_1](p^*) = -\mathbb{1}_\Sigma \mathbf{q}^*(0)$. Equation (3.4) writes

$$\frac{1}{\gamma}\Big(\mathbb{1}_\Sigma \mathbf{q}^*(0) - \varepsilon(p^* - \Delta p^*)\Big) \in \partial TV(p^*). \tag{3.6}$$

Finally, the first order optimality conditions are stated in the following result.

Theorem 3.2. *Fix K, Σ, $\varepsilon > 0$ and $\gamma > 0$. The function $p^* \in H_0^1(\Omega)$ is the optimal solution to (3.3) if and only if equation (3.6) is satisfied with $\mathbf{q}^*$ solution to (3.5) and $\mathbf{p}^*$ solution to (2.1) with p^* as initial condition.*

The optimality condition above is sufficient by a convexity argument.

Remark 3.2. *The computation of $\partial TV(p^*)$ is standard in a finite dimensional setting, either using a primal-dual algorithm or performing an approximation of $TV(p^*)$.*

3.3 Analysis of Problem (2.13)

We now focus on the *optimal design* problem (2.13). To perform the analysis, we give an equivalent formulation of $A_2(\mathbb{1}_\Sigma, p_0)$ using the particular form of $\mathbb{1}_\Sigma$. Indeed, for all $x \in \Sigma$, we will say that Γ is a subset of $\partial\Omega$ associated to $\Sigma \in \mathcal{U}_L$ whenever

$$\mathbb{1}_\Sigma(x) = \mathbb{1}_\Gamma(s + \mu\nu(s)) = \mathbb{1}_\Gamma(s), \qquad \text{for a.e. } x \in \widetilde{\partial\Omega},\ s \in \partial\Omega,\ \mu \in [0, \varepsilon] \tag{3.7}$$

for some $\mathbb{1}_\Gamma \in \mathcal{V}_L$ where $\mathbb{1}_\Gamma$ is the characteristic function of a subset Γ of $\partial\Omega$. Using Fubini-Tonelli-Lebesgue theorem, one has

$$\begin{aligned} A_2(\mathbb{1}_\Sigma, p_0) &= \frac{1}{\|p_0\|^2_{H^1(\Omega)}} \int_0^T \int_{\mathcal{B}} \mathbb{1}_\Sigma(x) \partial_t p_{[p_0]}(t,x)^2 \, dx \, dt \\ &= \frac{1}{\|p_0\|^2_{H^1(\Omega)}} \int_{\partial\Omega} \mathbb{1}_\Gamma(s) \psi_{[p_0]}(s) \, d\mathcal{H}^{d-1} \end{aligned} \tag{3.8}$$

where

$$\psi_{[p_0]}(s) = \int_0^T \int_0^\varepsilon \partial_t p_{[p_0]}(t, s + \mu\nu(s))^2 \, d\mu \, dt \tag{3.9}$$

Indeed, it follows directly from the regularity property of $p_{[p_0]}$ that $\psi_{[p_0]} \in L^1(\partial\Omega)$. Next theorem gives an existence result:

Theorem 3.3. *Let $\widetilde{p}_0 \in H^1(\Omega)$ be a solution of Problem (2.11). Then, the optimal design problem (2.13) has at least one solution. Moreover, there exists a real number λ such that Σ^* is a solution of (2.13) if and only if Σ^* is associated to Γ^* (in the sense of (3.7)) where*

$$\mathbb{1}_{\{\psi_{[\widetilde{p}_0]}(s) > \lambda\}} \leqslant \mathbb{1}_{\Gamma^*}(s) \leqslant \mathbb{1}_{\{\psi_{[\widetilde{p}_0]} \geqslant \lambda\}}(s), \qquad \textit{for a.e. } s \in \partial\Omega. \tag{3.10}$$

Proof. The proof is a direct adaptation of [28, Theorem 1]. It is based directly on the fact that the functional A_2 rewrites as (3.8), as well as a standard argument of decreasing rearrangement. Another convexity argument can be used to get this result, observing that the functional

$$\tilde{A}_2 : L^\infty(\partial\Omega, [0,1]) \ni \rho \mapsto \int_{\partial\Omega} \rho(s)\psi_{[p_0]}(s)\, d\mathcal{H}^{d-1}$$

is continuous for the weak-star topology of L^∞ and that the set

$$\mathcal{C}_L = \left\{ \rho \in L^\infty(\partial\Omega, [0,1]) \mid \int_{\partial\Omega} \rho = L\mathcal{H}^{d-1}(\partial\Omega) \right\}$$

is compact for this topology. It follows that the problem

$$\inf \left\{ \int_{\partial\Omega} \rho(s)\psi_{[p_0]}(s)\, d\mathcal{H}^{d-1},\ \rho \in \mathcal{C}_L \right\}$$

has at least one solution. Moreover, one shows easily that the solution can be chosen among the extremal points of the convex set $\mathcal{C}_L$, by using the convexity of the mapping $\tilde{A}_2$. □

3.4 Analysis of Problem (2.21)

This section is devoted to solving Problem (2.21) in the two-dimensional case, where the sensors set is the union of N_0 *similar* connected components (the definition of the sensors set has been made precise in (2.19)). Let us define

$$f_{[\widetilde{p}_0]} : \mathbb{T} \ni \theta \mapsto \psi_{[\widetilde{p}_0]}(\rho(\theta)\cos\theta, \rho(\theta)\sin\theta). \tag{3.11}$$

where $\psi_{[\widetilde{p}_0]}$ is given by (3.9).

Theorem 3.4. *Let $\widetilde{p}_0 \in H^1(\Omega)$ be a solution of Problem (2.11). Then, the optimal design problem (2.21) has at least a solution $\Sigma^{N_0,\ell}$. Let $\Gamma^{N_0,\ell}$ (resp. $(\theta_n)_{n\in\{1,\dots,N_0\}} \in \mathbb{T}^{N_0}$) be the associated set of $\partial\Omega$ in the sense of (2.14) (resp. the associated family of angles in the sense of (2.15)). Then,*

1. *if $N_0 = 1$, then, $f_{[\widetilde{p}_0]}(\theta_1) = f_{[\widetilde{p}_0]}(\hat{\theta}_1)$.*
2. *if $N_0 \geqslant 2$, let $n \in \{1, \dots, N_0 - 1\}$. One has the following alternative: either $\hat{\theta}_n = \theta_{n+1}$, or $f_{[\widetilde{p}_0]}(\theta_n) = f_{[\widetilde{p}_0]}(\hat{\theta}_n)$.*

If one assumes furthermore that ρ belongs to $C^2(\mathbb{T})$, then one has

$$\frac{f'_{[\widetilde{p}_0]}(\hat{\theta}_n)}{\sqrt{\rho(\hat{\theta}_n)^2 + \rho'(\hat{\theta}_n)^2}} - \frac{f'_{[\widetilde{p}_0]}(\theta_n)}{\sqrt{\rho(\theta_k n^2 + \rho'(\theta_n)^2}} \leqslant 0$$

whenever $N_0 = n = 1$ or $N_2 \geqslant 2$ and $n \in \{1, \dots, N_0 - 1\}$ is such that $\hat{\theta}_n < \theta_{n+1}$.

Proof. We first assume, without loss of generality that $N_0 \geqslant 2$, the case where $N_0 = 1$ being easily inferred by adapting the following reasoning. In what follows, we will use several times that $\rho(\theta) > 0$ for all $\theta \in \mathbb{T}$, which is a consequence of the fact that the point O (center of the considered orthonormal basis) belongs to the open set Ω.

First, using the same computations as those at the beginning of Section 3.3, we claim that Problem (2.21) can be recast as

$$\sup_{(\theta_1,\dots,\theta_{N_0})\in\Theta^{\ell}_{L,N_0}} J(\theta_1,\dots,\theta_{N_0}) \tag{3.12}$$

where

$$J(\theta_1,\dots,\theta_{N_0}) = \sum_{n=1}^{N_0} \int_{\theta_n}^{\hat{\theta}_n} f_{[\widetilde{p}_0]}(\theta)\sqrt{\rho(\theta)^2+\rho'(\theta)^2}\, d\theta, \tag{3.13}$$

with $f_{[\widetilde{p}_0]}$ defined by (3.11), $\hat{\theta}_n$ defined by (2.16) and

$$\Theta^{\ell}_{L,N_0} = \left\{ (\theta_1,\dots,\theta_{N_0}) \in \mathbb{T}^{N_0} \mid \int_{\theta_n}^{\theta_{n+1}} \sqrt{\rho(s)^2+\rho'(s)^2}\, ds \geqslant \ell,\ n = 1,\dots,N_0-1 \right\}. \tag{3.14}$$

Existence of a solution to this problem is standard and follows immediately from both the compactness of Θ^{ℓ}_{L,N_0} in $\mathbb{T}^{N_0}$ and the continuity of the functional. Let $(\theta_1,\dots,\theta_{N_0}) \in \Theta^{\ell}_{L,N_0}$ be a solution of the optimization problem (3.12). Let us assume the existence of $n \in \{1,\dots,N_0-1\}$ such that $\hat{\theta}_n < \theta_{n+1}$, in other words such that

$$\int_{\theta_n}^{\theta_{n+1}} \sqrt{\rho(s)^2+\rho'(s)^2}\, ds > \ell. \tag{3.15}$$

Then, it follows from the Karush-Kuhn-Tucker theorem that $\frac{\partial J}{\partial \theta_n}(\theta_1,\dots,\theta_{N_0}) = 0$, which rewrites

$$\sqrt{\rho(\theta_n)^2+\rho'(\theta_n)^2} f_{[\widetilde{p}_0]}(\theta_n) = f_{[\widetilde{p}_0]}(\hat{\theta}_n)\sqrt{\rho(\hat{\theta}_n)^2+\rho'(\hat{\theta}_n)^2}\frac{\partial \hat{\theta}_n}{\partial \theta_n}(\theta_n),$$

simplifying into

$$f_{[\widetilde{p}_0]}(\theta_n) = f_{[\widetilde{p}_0]}(\hat{\theta}_n), \tag{3.16}$$

by using that

$$\frac{\partial \hat{\theta}_n}{\partial \theta_n}(\theta_n) = \frac{\sqrt{\rho(\theta_n)^2+\rho'(\theta_n)^2}}{\sqrt{\rho(\hat{\theta}_n)^2+\rho'(\hat{\theta}_n)^2}}, \tag{3.17}$$

according to the combination of (2.16) with the implicit functions theorem. Furthermore, assuming that ρ is a C^2 function, the necessary second order optimality conditions write

$$\frac{\partial^2 J}{\partial \theta_n^2}(\theta_1,\dots,\theta_{N_0}) \leqslant 0,$$

which comes to

$$-\frac{\rho'(\theta_n)\left(\rho(\theta_n)+\rho''(\theta_n)\right)}{\sqrt{\rho(\theta_n)^2+\rho'(\theta_n)^2}}f_{[\widetilde{p}_0]}(\theta_n)-f'_{[\widetilde{p}_0]}(\theta_n)\sqrt{\rho(\theta_n)^2+\rho'(\theta_n)^2}$$
$$+\frac{\partial\hat{\theta}_n}{\partial\theta_n}(\theta_n)f'_{[\widetilde{p}_0]}(\hat{\theta}_n)\sqrt{\rho(\theta_n)^2+\rho'(\theta_n)^2}+\frac{\rho'(\theta_n)\left(\rho(\theta_n)+\rho''(\theta_n)\right)}{\sqrt{\rho(\theta_n)^2+\rho'(\theta_n)^2}}f_{[\widetilde{p}_0]}(\hat{\theta}_n)\leqslant 0 \quad (3.18)$$

Combining this inequality with both the optimality condition (3.16) and the relation (3.17) yield the desired result.

□

4 Numerical simulations

We are now interested in the numerical resolution of the problems according to the strategy provided by (2.11)-(2.13). However, as explained above, we will make some simplifications of the model for its numerical implementation.

We assume here that the sound speed $c(\cdot)$ is constant equal to 1. Since the aim is to validate the methodology introduced in the section 2.2, this simplification allows us to calculate in a simple way the solution of the Fourier space wave equation and thus obtain a high resolution in time and space.

Minimizing J^0 functional (Problem (2.11)) is carried out using a gradient splitting descent. More precisely, we alternate explicit processing of $A_1(1_\Sigma, p_0)$ via a time reversal imaging method [5, 13, 21, 22], with implicit processing of the term TV using the algorithm introduced by A. Chambolle in [14]. In addition, in practice, we also apply the FISTA strategy [10] to accelerate convergence.

With regard to determining the best position for the sensors Γ^*, we calculate the energy function $\psi_{[p_0]}$ defined for all $s \in \partial\Omega$ by

$$\psi_{[p_0]}(s)=\int_0^T \partial_t p_{[p_0]}(t,s)^2 dt.$$

• **For Problem** (2.13) **(continuous setting):** We apply Theorem 3.3, which shows that Γ^* should have the form

$$\Gamma^*_\lambda=\{s\in\partial\Omega \mid \psi_{[p_0]}(s)\geqslant\lambda\}.$$

It is also a simplification since $\psi_{[p_0]}$ is only observed on $\partial\Omega$ and the optimal constant λ is determined by using a dichotomy approach, looking for λ so that the constraint $\mathcal{H}^{d-1}(\Gamma^*_\lambda)=L\mathcal{H}^{d-1}(\partial\Omega)$is satisfied.

• **For Problem (2.21) (discrete setting, with a maximum number of connected components):** although Theorem 3.4 provides a partial characterization of the solution, we have observed numerically the existence of many local optima. For this reason, we have chosen to set up a genetic algorithm procedure. Precisely, we solve Problem (3.12) by using the Matlab© function `ga` designed to solve a finite dimensional optimization problem with a genetic algorithm. In practice, it is not worth taking into account the constraint (3.15) since it is naturally satisfied to the optimum.

We recall several standard results about *time reversal Imaging* in Section (4.1). In addition, in section (4.2), we show how the gradient of the functional $A_1(1_\Sigma, p_0)$ can be calculated using a generalized time reversal imaging technique. We also present a classical discretization of the wave equation (4.3) and its integration into Fourier space. Finally, we show some numerical illustrations of our approach in section 4.4, which highlights the improved reconstruction of the source p^0 when optimizing the position of the sensors.

4.1 Time reversal imaging

Recall that $p_{[p_0]}$ denotes the solution of Problem (2.1) for the initial datum p_0. If the given data p_{obs} are complete on the boundary of Ω i.e

$$p_{obs}(t,y) = p_{[p_0]}(t,y) \quad \text{for all } (t,y) \in [0,T] \times \partial\Omega,$$

then, the reconstruction of the initial source p_0 from data $g = p_{obs}$ can be done following time reversal imaging method, by using that

$$p_0(\cdot) \simeq \mathcal{I}[p_{obs}](\cdot) = w(T,\cdot),$$

where w is defined as the solution of the (backward) wave equation

$$\begin{cases} \partial_{tt} w(t,x) - \Delta w(t,x) = 0, & (t,x) \in [0,T] \times \Omega, \\ w(0,x) = \partial_t w(0,x) = 0, & x \in \Omega, \\ w(t,y) = p_{obs}(y, T-t), & t \in [0,T]. \end{cases}$$

More precisely, T is required to be sufficiently large to satisfy $u(T,\cdot) \simeq 0$ and $\partial_t u(T,\cdot) \simeq 0$ on Ω [21]. However, as explained in [5], the discretization of this imaging functional requires data interpolation on the boundary of Ω: this introduces smoothing effects on the reconstructed image (identical to the use of the penalization term $\mathcal{R}(p_0)$ in Problem (2.8)). In practice, it is more efficient to use an approximation version reading

$$\mathcal{I}[p_{obs}](x) = \int_0^T v_s(T,x)ds,$$

where v_s solves the wave equation

$$\begin{cases} \partial^2_{tt} v_s(t,x) - \Delta v_s(t,x) = \partial_t \left(\delta_{\{t=s\}} g(x, T-s)\right) \delta_{\partial\Omega}, & (t,x) \in \mathbb{R} \times \mathbb{R}^d \\ v_s(t,x) = 0, \quad \partial_t v_s(t,x) = 0, \quad x \in \mathbb{R}^d, t < s. \end{cases}$$

Here, $\delta_{\{t=s\}}$ denotes the time Dirac distribution at time $t = s$ and $\delta_{\partial\Omega}$ is the surface Dirac measure on the manifold $\partial\Omega$.

In particular, by using the so-called Helmholtz-Kirchhoff identity, it is proved in [3] that when Ω is close to a sphere with large radius in $\mathbb{R}^d$, there holds

$$p_0(x) \simeq \mathcal{I}[p_{obs}](x).$$

Another advantage of the modified time reversal imaging technique is its variational character. Indeed, recall that $p_{[p_0]}$ can be expressed as

$$p_{[p_0]}(\cdot) = \partial_t \mathbf{G}(t, \cdot) * p_0,$$

where $*$ is the convolution product in space, $\mathbf{G}$ the temporal Green function obtained as the inverse Fourier transform of G_ω

$$\mathbf{G}(t, \cdot) = \mathcal{F}_t^{-1}[G_\omega(\cdot)](t),$$

where G_ω denotes the outgoing fundamental solution to the Helmholtz operator $-(\Delta+\omega^2)$ in $\mathbb{R}^d$, that is the distributional solution of the equation

$$(\Delta + \omega^2)G_\omega(x) = -\delta_{\{x=0\}} \qquad x \in \mathbb{R}^d$$

subject to the outgoing Sommerfeld radiation equation

$$\lim_{|x|\to\infty} |x|^{\frac{d-1}{2}} \left(\frac{\partial}{\partial|x|} - i\omega\right) u(x) = 0.$$

The discrepancy functional A_1 defined by (2.9) can then be recast as

$$A_1(\mathbb{1}_\Sigma, p_0) = \frac{1}{2}\int_0^T \int_{\mathcal{B}} \mathbb{1}_\Sigma(y)((\partial_t \mathbf{G}(t, .) * p_0(.))(y) - p_{obs}(t, y))^2 dy\, dt.$$

Its Gâteaux-derivative with respect to the variable p_0, say

$$\langle dA_1(\mathbb{1}_\Sigma, p_0), h\rangle = \lim_{\tau\searrow 0} \frac{A_1(\mathbb{1}_\Sigma, p_0 + \tau h) - A_1(\mathbb{1}_\Sigma, p_0)}{\tau},$$

writes

$$\langle dA_1(\mathbb{1}_\Sigma, p_0), h\rangle = \int_\Omega \nabla A_1(\mathbb{1}_\Sigma, p_0)(x)h(x)\, dx,$$

where $\nabla A_1(\mathbb{1}_\Sigma, p_0)$ is the gradient with respect to p_0, identified to

$$\nabla A_1(\mathbb{1}_\Sigma, p_0) = \int_0^T \partial_t \mathbf{G}(t, .) * \left[(p_{[p_0]}(t, \cdot) - p_{obs}(t, \cdot))\mathbb{1}_\Sigma(\cdot)\right] dt$$

or

$$\nabla A_1(\mathbb{1}_\Sigma, p_0) = \int_0^T v_s(T, \cdot)\, ds, \tag{4.1}$$

where v_s solves

$$\begin{cases} \partial^2_{tt} v_s(t,x) - \Delta v_s(t,x) = \partial_t \left(\delta_{\{t=s\}} \left[p_{[p_0]}(T-s,\cdot) - p_{obs}(T-s,\cdot) \right] \right) \mathbb{1}_\Sigma(\cdot), \\ v_s(t,x) = 0, \quad \partial_t v_s(t,x) = 0, \quad x \in \mathbb{R}^d, t < s. \end{cases}$$

This claim follows from an straightforward adaptation of the proof of Theorem 3.2. In particular, the gradient $\nabla A_1(\mathbb{1}_\Sigma, p_0)$ corresponds to the modified time reversal imaging associated to the data $p_{[p_0]} - p_{obs}$, where the Dirac mass $\delta_{\partial\Omega}$ is replaced by the characteristic function $\mathbb{1}_\Sigma$ and

$$\nabla A_1(\mathbb{1}_\Sigma, p_0) = \mathcal{I}[p_{[p_0]} - p_{obs}].$$

4.2 Solving Problem (2.11)

In this section, we focus on numerical algorithms to solve Problem (2.11). Because of the smoothing effects mentioned in Section 4.1, it is not worth to add a H^1-penalization term from a practical point of view. This is why we eventually consider that

$$J^0(\mathbb{1}_\Sigma, p_0) = A_1(\mathbb{1}_\Sigma, p_0) + \gamma TV(p_0).$$

A first idea is to use a gradient-iterative scheme with an implicit treatment of the TV norm, combined with an explicit treatment of $A_1(1_\Sigma, p_0)$. In this context, the simplest iterative scheme is the forward-backward algorithm, reading

$$p_0^{n+1} = (I + \eta\gamma\partial TV)^{-1}(p_0^n - \eta \nabla A_1(\mathbb{1}_\Sigma, p_0^n)), \qquad n \geqslant 0,$$

where $p^0 = 0$ and η is a given (small positive) descent step. The TV proximal operator $\text{prox}_{\eta TV}[u]$ is defined by

$$\text{prox}_{\eta TV}[u] = (I + \eta\partial TV)^{-1}(u) = \underset{v \in L^2(\mathcal{B})}{\text{argmin}} \left\{ \frac{1}{2\eta} \|u - v\|^2_{L^2(\mathcal{B})} + TV(v) \right\}.$$

is computed by using the dual approach introduced by Chambolle in [14].

Finally, the gradient $\nabla A_1(\mathbb{1}_\Sigma, p_0)$ is computed via a time reversal imaging approach. Indeed, $\nabla A_1(\mathbb{1}_\Sigma, p_0)$ given by (4.1) can also be expressed (using the superposition principle) as $\nabla A_1(\mathbb{1}_\Sigma, p_0) = v_s(T, \cdot)$, with

$$\begin{cases} \partial^2_{tt} v_s - \Delta v_s = F, \quad (t,x) \in \mathbb{R}^+ \times \mathbb{R}^d, \\ v_s(0,x) = 0 = \partial_t v_s(0,x) = 0, \quad x \in \mathbb{R}^d, \end{cases}$$

where the right hand-side term is the measure

$$F = \partial_t \left(\delta_{\{t=s\}} \left[p_{[p_0]}(T-s,\cdot) - p_{obs}(T-s,\cdot) \right] \right) \mathbb{1}_\Sigma.$$

4.3 Time reversal Imaging, wave equation and discretization

Recall that the direct problem and the time reversal imaging approach only require to solve a Cauchy wave equation on the form

$$\begin{cases} \partial_{tt}^2 v_s(t,x) - \Delta v_s(t,x) = F(t,x), \quad (t,x) \in \mathbb{R}^+ \times \mathbb{R}^d, \\ v_s(0,x) = H_1(x), \quad \partial_t v_s(0,x) = H_2(x), \quad x \in \mathbb{R}^d, \end{cases}$$

Comments on numerics. With regard to numerical discretization, all wave-like equations are solved in in the box $\mathcal{B} = [-D/2, D/2]^2$ with periodic boundary conditions, where D is supposed to be large enough to prevent any reflection on the boundary. The numerical integrations of each equation are then performed exactly in Fourier space.

We recall that the Fourier truncation of a two-dimensional function u to the M first modes, in a box $\mathcal{B} = [-D/2, D/2]^2$ is given by

$$u^M(t,x) = \sum_{n_1,n_2=-[M/2]}^{[M/2]} c_{\mathbf{n}}(t) e^{2i\pi\xi_{\mathbf{n}}\cdot x}$$

where $\mathbf{n} = (n_1, n_2)$, $\xi_{\mathbf{n}} = (n_1/D, n_2/D)$ and $[\cdot]$ stands for the integer part function. Here, the coefficients $c_{\mathbf{n}}$ stand for the $(2[M/2])^2$ first discrete Fourier coefficients of u. In addition, we use the inverse fast Fourier transform (denoted $IFFT$) to compute the inverse discrete Fourier transform of $c_{\mathbf{n}}$. This leads to $u_{\mathbf{n}}^M = IFFT[c_{\mathbf{n}}]$ where $u_{\mathbf{n}}^M$ is the value of u at the points $x_{\mathbf{n}} = (n_1 h, n_2 h)$ where $h = D/M$.
Conversely, $c_{\mathbf{n}}$ can be computed by applying the discrete Fourier transform to $u_{\mathbf{n}}^M$:

$$c_{\mathbf{n}} = FFT[u_{\mathbf{n}}^M].$$

Now, about computation of wave equation solutions, remark that a generic wave equation

$$\partial_{tt}^2 u^M(t,x) - \Delta u^M(t,x) = F^M(t,x) = \sum_{n_1,n_2=-M/2}^{M} f_{\mathbf{n}}(t) e^{2i\pi\xi_{\mathbf{n}}\cdot x}$$

reads

$$\partial_t \begin{pmatrix} u^M \\ u_t^M \end{pmatrix} = \begin{pmatrix} 0 & I_d \\ \Delta & 0 \end{pmatrix} \begin{pmatrix} u^M \\ u_t^M \end{pmatrix} + \begin{pmatrix} 0 \\ F^M \end{pmatrix}$$

which can by simply integrated by solving the linear EDO system

$$\frac{d}{dt} \begin{pmatrix} c_{\mathbf{n}}(t) \\ c'_{\mathbf{n}}(t) \end{pmatrix} = \begin{pmatrix} 0 & 1 \\ -4\pi^2|\xi_{\mathbf{n}}|^2 & 0 \end{pmatrix} \begin{pmatrix} c_{\mathbf{n}}(t) \\ c'_{\mathbf{n}}(t) \end{pmatrix} + \begin{pmatrix} 0 \\ f_{\mathbf{n}}(t) \end{pmatrix}.$$

4.4 Numerical experiments

All the numerical simulations of this section are done with the following set of parameters:

- the set Ω is a two-dimensional ball of radius 1
- the box $\mathcal{B} = [-D/2, D/2]^d$ has size $D = 4$ and the record time is $T = 2$;
- the set K is a two-dimensional ball of radius 0.85
- we use a regular time step discretization $dt = T/2^{10}$ and $dx = D/2^9$.
- the thickness parameter ε is equal to 0.03.
- the TV-parameter $\gamma = 0.01$.
- the descent step $\eta = 0.5$.

To avoid inverse crime [15, 32], we also use two different grids to compute the solution of the direct and inverse problem: the direct data g are then computed on a grid two times smaller, namely $dx = D/2^{10}$.

On Figure 4.1, we provide a first experiment using ideal complete data $g = p_{obs}$ on the whole boundary $\partial\Omega$ as well as the time reversal imaging $\mathcal{I}(g)$ for three different values of the pressure p_0. It is observed that in each case, the reconstructed source and the exact source are very close.

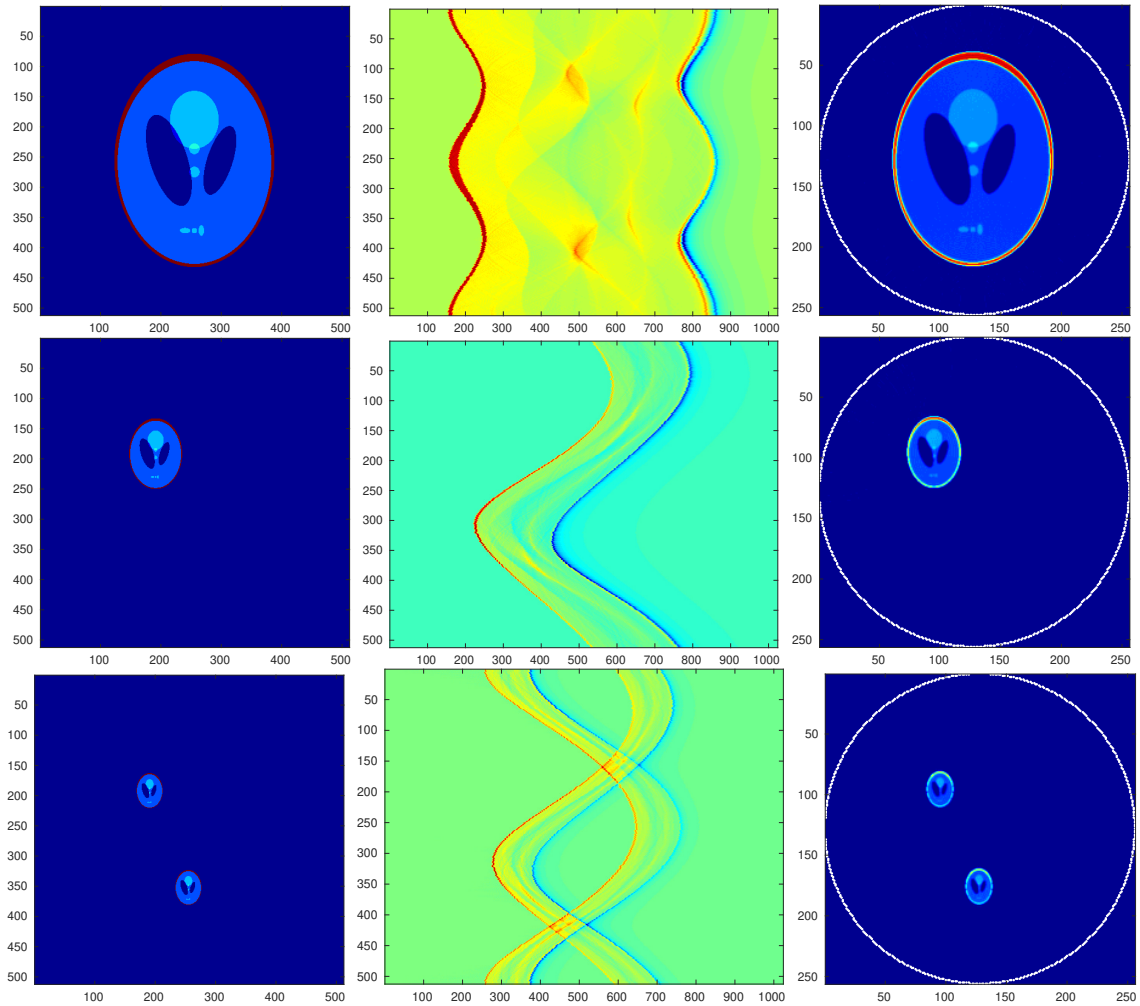

Figure 4.1: Source reconstruction using time reversal imaging $\mathcal{I}$. Each line corresponds to a different choice of the source p_0. Left: initial source p_0; middle: data $g = p_{obs}$; right: $\mathcal{I}[g]$. The white dots corresponds to sensors positions.

On Figure 4.2, we give the result of the reconstruction procedure described in section 2.2 using partial data $g = p_{obs}$ with $L = 0.3$. To test its effectiveness, we also added 5% of noise on the data g. The position of sensors is plotted with white marks on each picture. Each line corresponds to a different choice of the source p_0: we have plotted the source p_0, the result of the reconstruction using the time reversal imaging p_0^0 and the reconstruction of the source p_0^n after $n = 30$ iterations. In particular, we observed that some information on p_0 are lost and in particular the discontinuities with normal directions that do not meet any sensor.

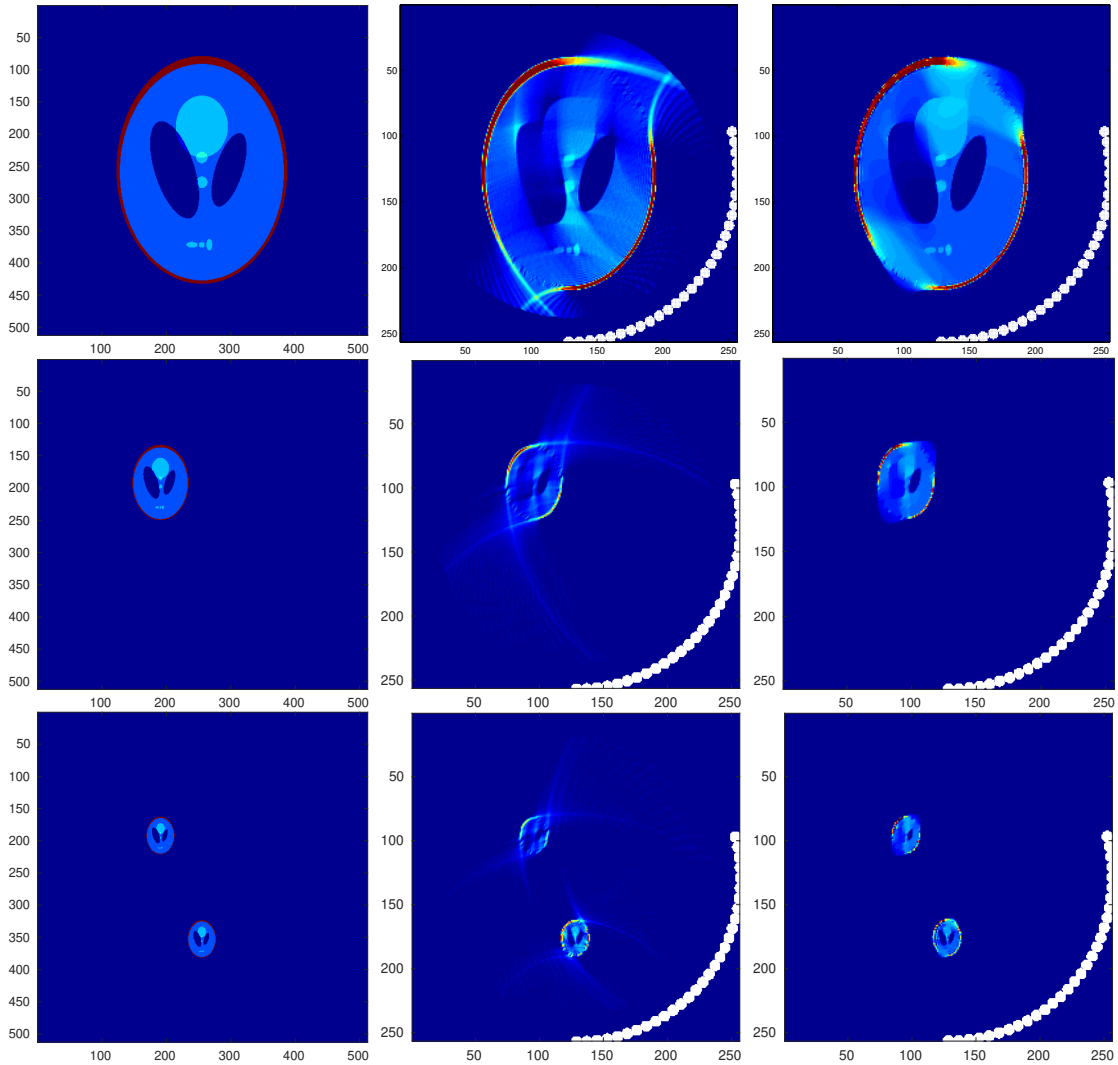

Figure 4.2: Minimization of J^0 w.r.t. $(\mathbb{1}_\Sigma, p_0)$. Each line corresponds to a different choice of the source p_0. Left: initial source p_0; middle: reconstruction using time reversal imaging-$\mathcal{I}[g]$; right: reconstructed source p_0^n after $n = 30$ iterations. The white dots correspond to sensors positions.

Next, on Figure 4.3, we present the reconstruction of the source p_0 if one allows the sensors position to evolve. As previously, each line corresponds to a different choice of the source p_0. Moreover, on each line, we respectively plotted

- the reconstructed source p_0^n after $n = 30$ iterations,
- the energy function $\psi_{u[p_0^n]}$ computed on Ω and the associated optimal position of sensors plotted with red marks.

- the reconstructed source p_0^n after $n = 15$ iterations after using the new position of sensors.

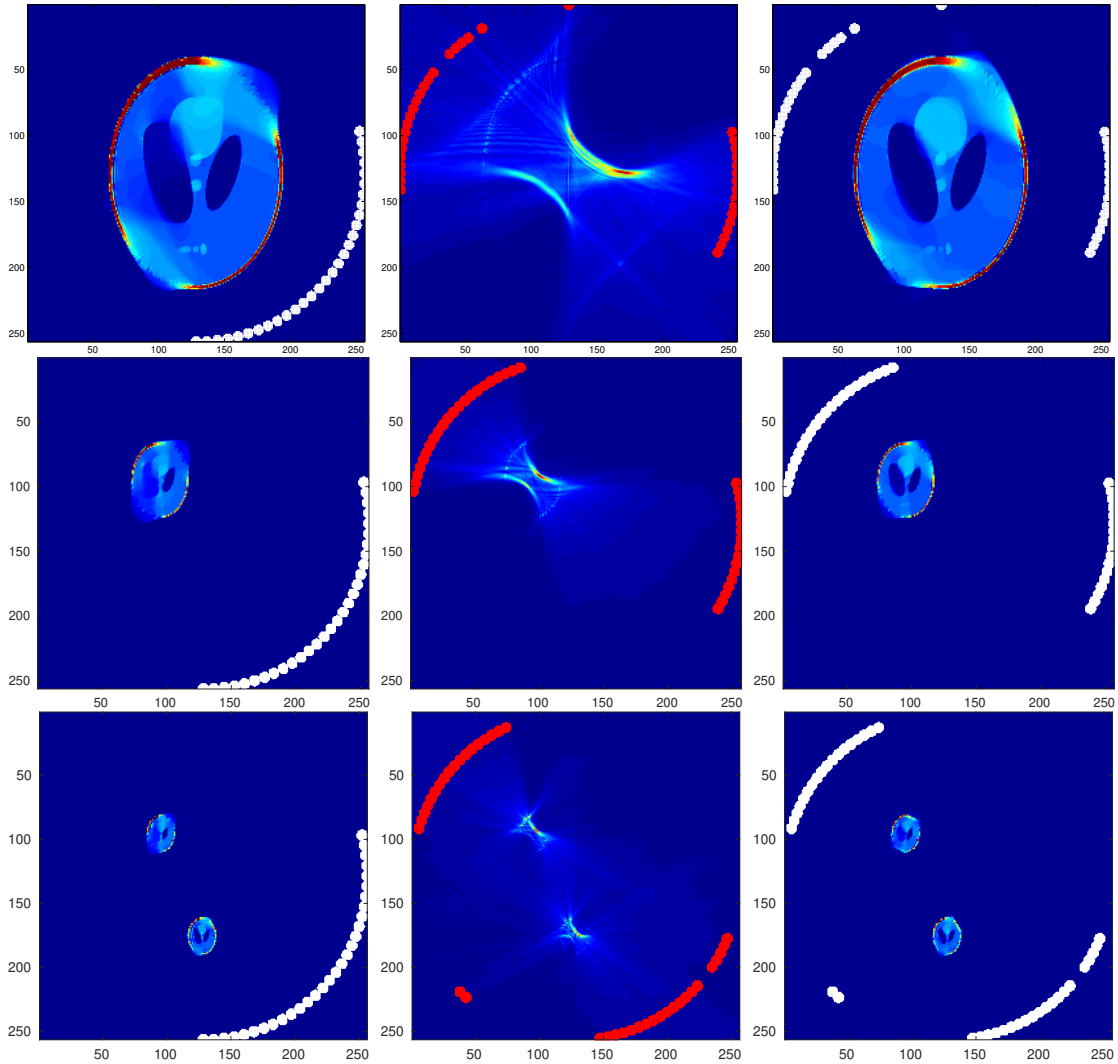

Figure 4.3: Optimization of sensors position. Each line corresponds to a different choice of the source p_0; Left: reconstructed source p_0^n after $n = 30$ iterations by using initial positions of the sensors; middle: function $\psi_{p_0^n}$ defined by (3.9) on Ω and new position of sensors (*red* dots); right: reconstructed source p_0^n after $n = 20$ iterations by using the new position of sensors.

Finally, as expected, the reconstruction of the source is much better by using the new position of sensors even if, the reconstruction remains unperfect.

We present now an illustration of the influence of the initial location of the sensors on our procedure. On Fig. 4.4, we present several numerical experiments where each line corresponds to a different value of the initial location. As with previous simulations, we observe that the reconstruction of the source is much better by using the new position of the sensors. As for choosing a good initial position, it is not an easy task, especially since we do not have any a priori information on the source.

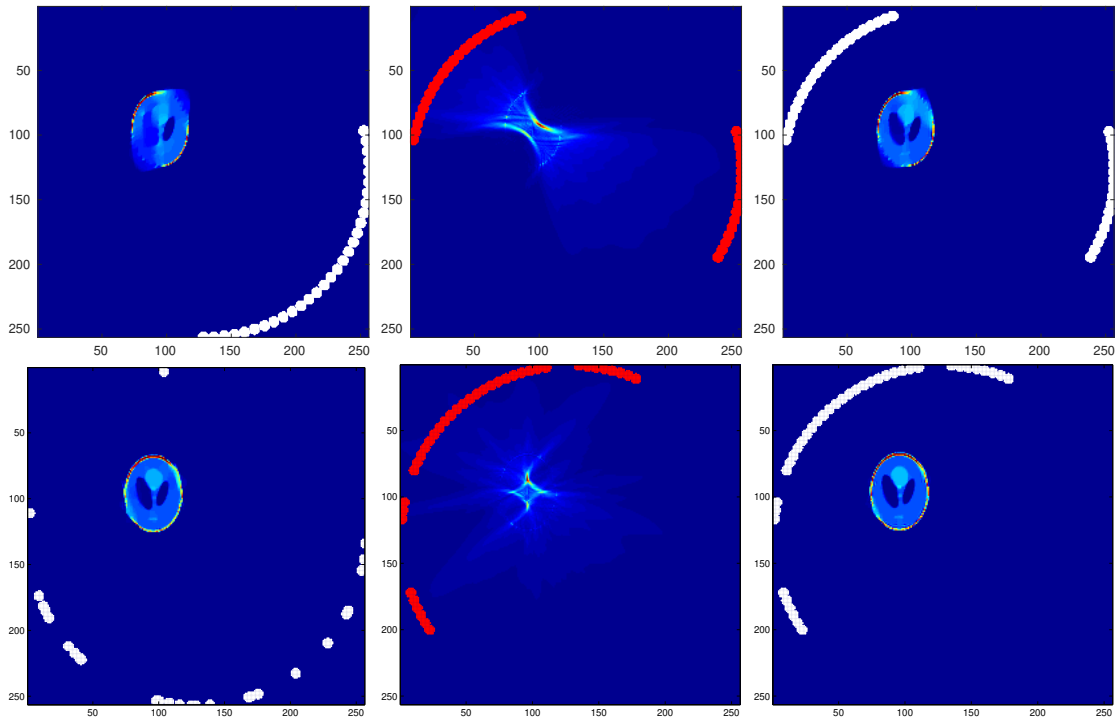

Figure 4.4: Optimization of sensors position : influence of the initial position of sensors. Each line corresponds to a different choice of the initial location of the sensors ; Left: reconstructed source p_0^n after $n = 30$ iterations by using initial positions of the sensors; middle: function $\psi_{p_0^n}$ defined by (3.9) on Ω and new position of sensors (*red* dots); right: reconstructed source p_0^n after $n = 20$ iterations by using the new position of sensors.

Let us illustrate the interest of using the term A_2 as a good reconstruction quality factor. On Figures 4.5 and 4.6, we first compute the optimal position of sensors, respectively in the continuous and discrete[1] settings, using the true value of the source term p_0. Second, using the new sensors position, we provide an estimate of the source p_0 by solving Problem (2.11). In each case, we observe that the source reconstruction is almost perfect.

[1]Meaning that we consider a given number of sensors.

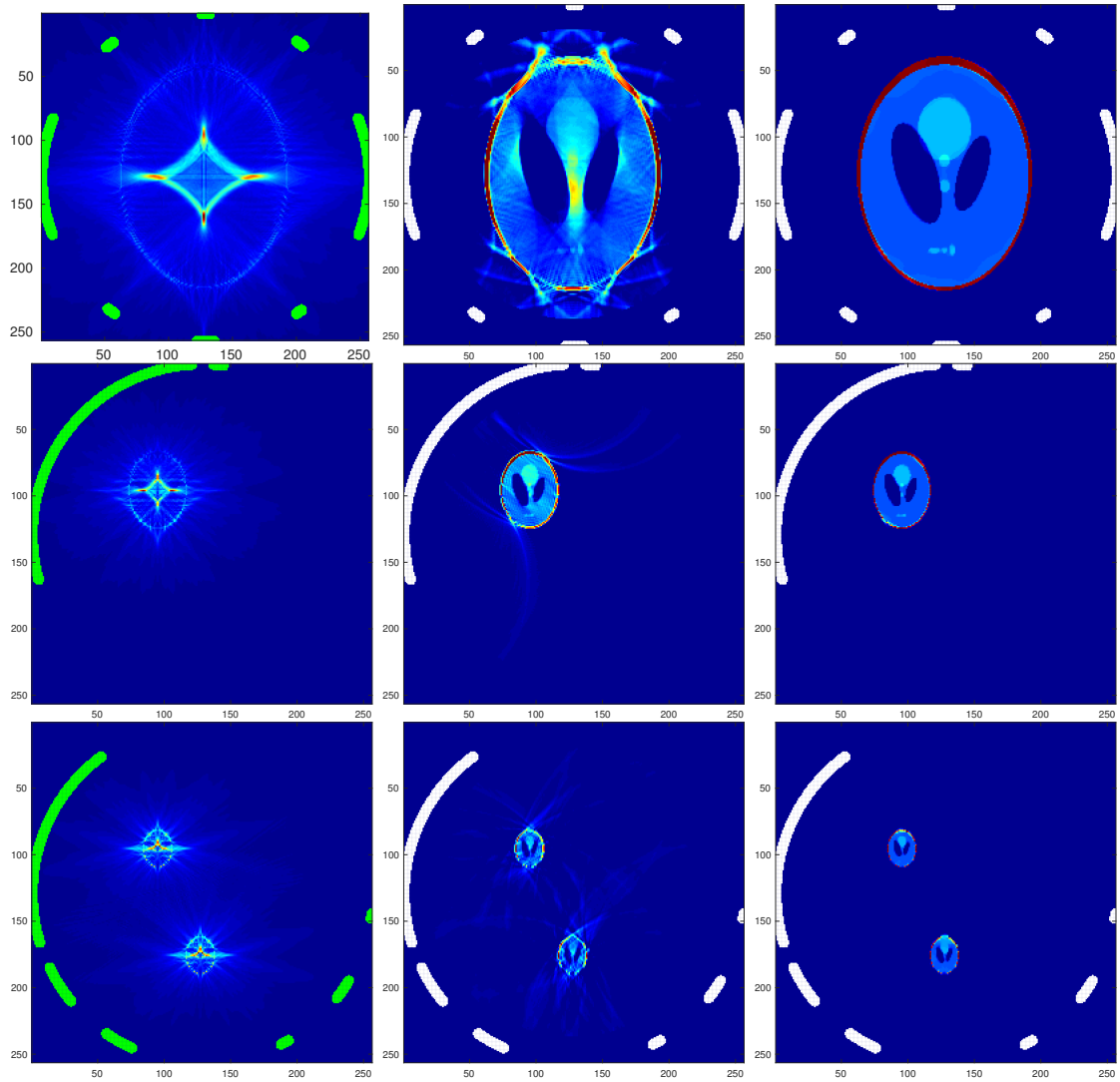

Figure 4.5: Optimization of sensors position. Each line corresponds to a different choice of the source p_0. Left: function $\psi_{[p_0]}(x)$ defined by (3.9) on Ω and the best position of sensors (green dots); middle: reconstruction by using the time reversal imaging $\mathcal{I}[g]$; right: reconstructed source p_0^n after $n = 30$ iterations by using the resulting optimal position of sensors.

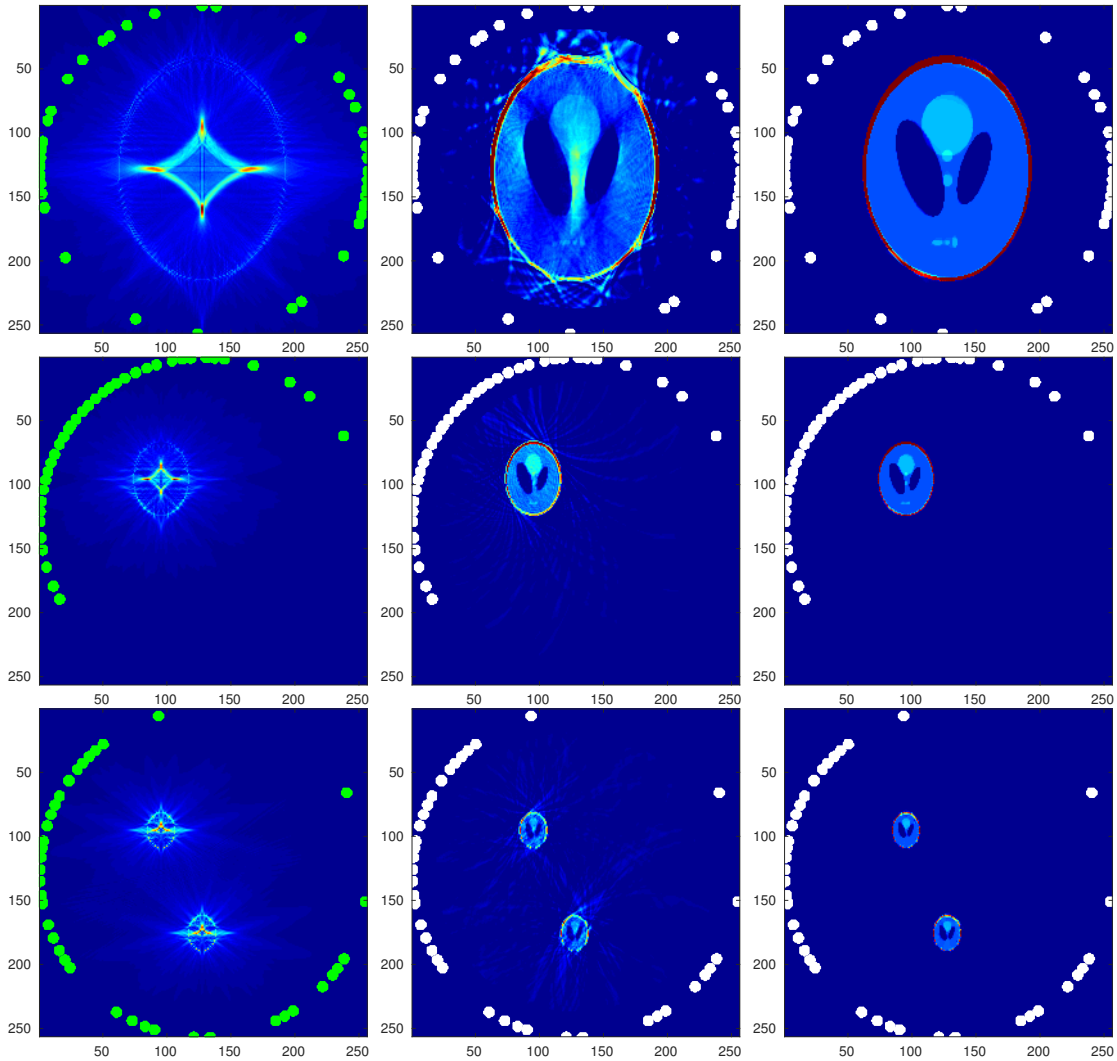

Figure 4.6: Optimization of sensors position with only 38 sensors. Each line corresponds to a different choice of the source p_0. Left: function $\psi_{[p_0]}(x)$ defined by (3.9) on Ω and the best position of sensors (green dots); middle: reconstruction by using the time reversal imaging $\mathcal{I}[g]$; right: reconstructed source p_0^n after $n = 30$ iterations by using the resulting optimal position of sensors.

5 Conclusion

This article is a first attempt to efficiently locate sensors in the highly sensitive context of thermo-acoustic tomography. While the first numerical results appear promising, we plan to investigate this issue further by examining the following elements

- other modeling choices. In particular, are there better choices of functional A_2 as quality factors for reconstruction (e.g. other observers)?
- how to choose more appropriately the term regularization in the optimization problem and study the sensitivity of the solution to this term?
- will the iterative scheme of successively estimating the source p_0 and then a new position of the sensors converge? In this case, can the limit be identified?
- can we analyze the relationships between the reconstruction parameters and the number of sensors used for the experiment?
- how to improve the optimization procedure, especially when it comes to a finite number of sensors for which we use an efficient but expensive genetic algorithm?
- could the reconstruction be improved if one is able to rotate the sensors freely around the target? Indeed, a first refinement of the method introduced in the present article could read as follows: *fix N sensors. Compute the best location. Perform $k-1$ rotations to get kN measurements and go to next step to find the new best location with kN sensors.* However, this issue needs to be more thorough and thoughtful, taking into account its practical implementation and possibly proposing a dedicated reconstruction algorithm.

More generally, we also plan to collaborate with physics researchers to conduct experiments and test our approach and method on real medical imaging data. We believe that the techniques developed in this article can be adapted to many other situations. Nevertheless, it is likely that several additional constraints on the sensor set must be taken into account, usually a restriction on the sensor position areas.

References

[1] H. Akhouayri, M. Bergounioux, A. Da Silva, P. Elbau, A. Litman, and L. Mindrinos. Quantitative thermoacoustic tomography with microwaves sources. *Journal of Inverse and Ill Problems*, 2017.

[2] H. Ammari. An inverse initial boundary value problem for the wave equation in the presence of imperfections of small volume. *SIAM J. Control Optim.*, 41(4):1194–1211, 2002.

[3] H. Ammari. *An introduction to mathematics of emerging biomedical imaging*, volume 62. Springer, 2008.

[4] H. Ammari, E. Bossy, V. Jugnon, and H. Kang. Mathematical modeling in photoacoustic imaging of small absorbers. *SIAM Rev.*, 52(4):677–695, 2010.

[5] H. Ammari, E. Bretin, J. Garnier, and A. Wahab. Time reversal in attenuating acoustic media. In *Mathematical and statistical methods for imaging*, volume 548 of *Contemp. Math.*, pages 151–163. Amer. Math. Soc., Providence, RI, 2011.

[6] H. Ammari and H. Kang. *Reconstruction of small inhomogeneities from boundary measurements*. Number 1846. Springer Science & Business Media, 2004.

[7] S. R. Arridge. Optical tomography in medical imaging. *Inverse Problems*, 15(2), 1999.

[8] G. Bal, K. Ren, G. Uhlmann, and T. Zhou. Quantitative thermo-acoustics and related problems. *Inverse Problems*, 27(5):055007, 15, 2011.

[9] G. Bal and G. Uhlmann. Inverse diffusion theory of photoacoustics. *Inverse Problems*, 26(8):085010, 20, 2010.

[10] A. Beck and M. Teboulle. A fast iterative shrinkage-thresholding algorithm for linear inverse problems. *SIAM J. Imaging Sci.*, 2(1):183–202, 2009.

[11] M. Bergounioux, X. Bonnefond, T. Haberkorn, and Y. Privat. An optimal control problem in photoacoustic tomography. *Mathematical Models and Methods in Applied Sciences*, 24(12):2525–2548, 2014.

[12] X. Bonnefond. *Contributions à la tomographie thermoacoustique. Modélisation et inversion*. PhD thesis, Université de Toulouse, Université Toulouse III-Paul Sabatier, 2010.

[13] E. Bretin, C. Lucas, and Y. Privat. A time reversal algorithm in acoustic media with dirac measure approximations. *Inverse Problems*, 34(4):045004, 2018.

[14] A. Chambolle. An algorithm for total variation minimization and applications. *J. Math. Imaging Vision*, 20(1-2):89–97, 2004. Special issue on mathematics and image analysis.

[15] D. Colton and R. Kress. *Inverse acoustic and electromagnetic scattering theory*, volume 93 of *Applied Mathematical Sciences*. Springer, New York, third edition, 2013.

[16] R. Dautray and J.-L. Lions. *Mathematical analysis and numerical methods for science and technology*, volume 5. Springer, 1993.

[17] E. Demidenko, A. Hartov, N. Soni, and K. D. Paulsen. On optimal current patterns for electrical impedance tomography. *IEEE Transactions on Biomedical Engineering*, 52(2):238–248, Feb 2005.

[18] I. Ekeland and R. Temam. *Convex Analysis and Variational Problems*. Classics in Applied Mathematics. Society for Industrial and Applied Mathematics (SIAM, 3600 Market Street, Floor 6, Philadelphia, PA 19104), 1999.

[19] L. C. Evans. *Partial differential equations*, volume 19 of *Graduate Studies in Mathematics*. American Mathematical Society, Providence, RI, 1998.

[20] H. Garde and S. Staboulis. Convergence and regularization for monotonicity-based shape reconstruction in electrical impedance tomography. *Numer. Math.*, 135(4):1221–1251, 2017.

[21] Y. Hristova. Time reversal in thermoacoustic tomography—an error estimate. *Inverse Problems*, 25(5):055008, 14, 2009.

[22] Y. Hristova, P. Kuchment, and L. Nguyen. Reconstruction and time reversal in thermoacoustic tomography in acoustically homogeneous and inhomogeneous media. *Inverse Problems*, 24(5):055006, 25, 2008.

[23] N. Hyvönen, A. Seppänen, and S. Staboulis. Optimizing electrode positions in electrical impedance tomography. *SIAM J. Appl. Math.*, 74(6):1831–1851, 2014.

[24] M. Neumayer, M. Flatscher, T. Bretterklieber, and S. Puttinger. Optimal design of ect sensors using prior knowledge. *Journal of Physics: Conference Series*, 1047(1):012012, 2018.

[25] S. K. Patch and O.Scherzer. Photo- and thermo-acoustic imaging introduction. *Inverse Problems*, 23:1–10, 2017.

[26] Y. Privat, E. Trélat, and E. Zuazua. Optimal location of controllers for the one-dimensional wave equation. *Ann. Inst. H. Poincaré Anal. Non Linéaire*, 30(6):1097–1126, 2013.

[27] Y. Privat, E. Trélat, and E. Zuazua. Optimal observation of the one-dimensional wave equation. *J. Fourier Anal. Appl.*, 19(3):514–544, 2013.

[28] Y. Privat, E. Trélat, and E. Zuazua. Complexity and regularity of maximal energy domains for the wave equation with fixed initial data. *Discrete Contin. Dyn. Syst. Ser. A*, 35(12):6133–6153, 2015.

[29] Y. Privat, E. Trélat, and E. Zuazua. Optimal shape and location of sensors for parabolic equations with random initial data. *Archive for Rational Mechanics and Analysis*, 216(3):921–981, 2015.

[30] Y. Privat, E. Trélat, and E. Zuazua. Optimal observability of the multi-dimensional wave and Schrödinger equations in quantum ergodic domains. *J. Eur. Math. Soc. (JEMS)*, 18(5):1043–1111, 2016.

[31] O. Scherzer, M. Grasmair, H. Grossauer, M. Haltmeier, and F. Lenzen. *Variational Methods in Imaging*. Springer, 2008.

[32] A. Wirgin. The inverse crime. In *LMA/CNRS, 31 chemin Joseph Aiguier, 13402 Marseille cedex 20*.

[33] L. Xu, M.and Wang. Photoacoustic imaging in biomedecine. *Rev. Sci. Instrum.*, 77(4), 2006.

[34] W. Yan, S. Hong, and R. Chaoshi. Optimum design of electrode structure and parameters in electrical impedance tomography. *Physiological Measurement*, 27(3):291, 2006.